Can the shock wave generated by the thermal runaway of a lithium-metal all-solid-state cell be predicted by material-scale analysis

Juliette Charbonnel, Alain Bengaouer, Pierre-Xavier Thivel, Rémi Vincent

Title:

Can the shock wave generated by the thermal runaway of a lithium-metal all-solid-state cell be predicted by material-scale analysis

Authors:

Juliette Charbonnel[a,b], Alain Bengaouer[b], Pierre-Xavier Thivel[a] and Rémi Vincent [b,]*

Email: remi.vincent@cea.fr

[a] University Grenoble Alpes, University Savoie Mont Blanc, CNRS, Grenoble INP, LEPMI, F-38000 Grenoble, France

[b] University Grenoble Alpes, CEA, LITEN, DEHT, F-38000 Grenoble, France

Keywords:

All-solid-state battery; thermal runaway; model; blast wave; TGA; DSC.

Key points:

- The safety of the Li|LLZO|NMC811 cell has been assessed numerically.
- A thermal runaway model has been developed from material scale analysis.
- This model is in line with cell-scale experiments and is therefore validated.
- The safety of the anode less Li|LLZO|NMC811 cell has been predicted.

Abstract:

It is widely believed that all-solid-state batteries would be safer than traditional Li-ion ones. This study develops a thermal runaway model for lithium-metal all-solid-state cells. First, material-scale analysis were carried out to determine model parameters. Then, they were used to simulate the thermal runaway in a closed calorimeter. The initiation temperature, the energy released by the thermal runaway and its duration are consistent with the experimental data. Additionally, the model simulates the overpressure produced by this thermally abused cell in an open system and showing strong correlation with experimental data. After validation, the model was used to predict the thermal runaway of an anode-less lithium-metal all-solid-state

battery. Even with the minimum quantity of lithium, the thermal runaway, while reduced, remained significant. Moreover, this work highlights the impact of the oxygen released, its strong reaction with the lithium during TR and the subsequent blast wave overpressure caused by the generated gases.

Introduction:

Wind and photovoltaic energies are by nature intermittent and contribute only up to 10% of global electricity production. The development of these renewable energies requires efficient and cost-effective energy storage solutions. Lithium-ion batteries (LiBs) can contribute significantly to renewable energy storage, furthermore the integration of LiBs in electronic devices and electric vehicles is an attractive solution due to their high mass and volumetric energy density. However, safety issues raised by the thermal runaway (TR) of current LiBs hinder their wide adoption.

LiB are made up of two electrodes. A negative electrode usually made of graphite with a current collector made of copper. In addition, LiB have a positive electrode, which is a metallic mixed oxide such as $Li_xNi_{0.8}Mn_{0.1}Co_{0.1}O_2$ (NMC811) with a current collector made of aluminium [1]. LiB are also composed of a polymer separator and a liquid electrolyte (organic solvents + salt) [1]. Finally, LiB have an interphase between the negative electrode and the liquid electrolyte called the solid electrolyte interphase (SEI). The polymer separator, the liquid electrolyte and the SEI are considered the most dangerous components during thermal runaway (TR) [2]. There is also an exothermic reaction between the lithiated graphite and the liquid electrolyte.

TR can been defined as an exothermic reaction, which goes out of control [3]. The temperature increases and causes a reaction rate which leads to a further temperature increase until no oxidizer (O_2) or combustible (Li and/or organic products) remains. When TR occurs, smoke, fire and sometimes explosions can be observed [4].

All-solid-state battery (ASSB) technology could increase battery safety because the polymer separator and the liquid electrolyte are replaced by a solid electrolyte (SE) [5]. The SE can be made of ceramic such as $Li_7La_3Zr_2O_{12}$ (LLZO) or glass such as

Li_6PS_5Cl (LPSCl) [6]. Another point in favour of ASSB is to increase the energy density by replacing the lithiated graphite negative electrode with a lithium-metal foil [7,8]. In the same way, to increase battery energy density, nickel-rich metallic oxides are used as a positive electrode in the ASSB [9]. However, this technology is under development. The main reason is that every SE has at least one major defect which prevents it from being viable [7]. At present, ASSBs at several ampere hours are not commercialized. Therefore, their safety cannot be assessed on real-scale cells (over $1\ \mathrm{Ah}$).

Nevertheless, several authors have assessed ASSB safety based on studies at the material scale. Differential Scanning calorimetry (DSC) analyses have been performed on LiB and ASSB microcells. When the positive electrode has a spinel structure, the reaction enthalpy is about $450\ \mathrm{kJ.mol^{-1}}$ for LiB and $150\ \mathrm{kJ.mol^{-1}}$ for ASSB [10]. This paper presents a method for achieving greater safety thanks to the use of an SE. However, it simultaneously modifies two parameters: the electrolyte (liquid or solid) and the cathode material (NCA/NMC or LCO). It is difficult to determine which change has the greatest influence on enthalpy decrease. Furthermore, ultimate safety has not yet been achieved. In two other papers, accelerating rate calorimetry (ARC) was used to assess the safety of stacking Li|SE|Li [11,12]. Severe TR occurs when stacking with polymer electrolytes: $Li_{1.5}Al_{0.5}Ge_{1.5}(PO_4)_3$ (LAGP), $Li_{1.4}Al_{0.4}Ti_{1.6}(PO_4)_3$ (LATP), Li_3PS_4, $Li_7P_3S_{11}$, Li_4SnS_4,$Li_{9.4}Si_{1.74}P_{1.44}S_{11.7}Cl_{0.3}$ (LiSiPSCl) and LPSCl. For the stacking with $Li_{3x}La_{2/3-x}TiO_3$ (LLTO) a slight reaction occurs. Finally, no reaction is observed when stacking with Ta-doped LLZO [11,12]. The solid electrolyte chosen can influence the thermal stability of the ASSB. In a recent paper, a bulk-type cell was composed of Li|LPSCl|NMC811 gently ground using a mortar and a pestle. When the cell was charged to 4.4 and $4.5\ \mathrm{V}$ (vs Li^+/Li), it burned

violently at $150\ °C$ with flames [13]. These studies call into question the ultimate safety of ASSB. However, the main limitation of these experimental studies is their small scale so the extrapolation of these results to a real ASSB cell is uncertain.

Another way to assess ASSB safety is by modelling. A thermodynamic model has been built to determine the heat released by an ASSB under different failure scenarios. Under short circuit abuse, ASSB and LiB released the same amount of heat: $14\ \mathrm{J.mAh^{-1}}$ [14]. In the case of a catastrophic SE failure, ASSB released $8\ \mathrm{J.mAh^{-1}}$ [14]. This thermodynamic model showed that TR could occur for an ASSB in both scenarios. Furthermore, the specific heat capacity (c_p) was lower for an ASSB than for a LiB one. By decreasing the cell specific heat capacity, the adiabatic temperature rose during TR [15]. Therefore, ASSB should have a higher adiabatic temperature than LiB. A 2D TR model was built with a $Li|$ Na-doped LLZO $|Li_{0.47}CoO_2$ (LCO) cell. The reactions taken into account by the model were lithium fusion, the destabilization of the positive electrode (LCO) which led to the release of O_2 and the formation of Li_2O. TR occured for this cell with SE. The initiation temperature (T_{ini}) and maximum temperature (T_{max}) were about 320 and $1{,}000\ °C$ [15]. For a LiB with graphite and LCO as electrodes, T_{ini} and T_{max} are respectively $226\ °C$ and $639\ °C$ [16]. As expected, the rise in ASSB adiabatic temperature was higher than that of the LiB. The ultimate safety of ASSB can be questioned by these modelling studies. The main limitations of these models are the lack of experimental validation at the cell level, and the input data mainly taken from the literature. To overcome these limitations, in this study a specific approach has been developed (Figure 1). At the material scale, DSC is carried on NMC811 powder alone or in contact with a lithium-metal foil. NMC811 was previously loaded to a state of charge (SOC) of 100 %. Kinetics parameters: pre-exponential factor (A), energy activation (E_a) and enthalpy of reaction (ΔH) were deduced from

these analyses. A and E_a were determined using Kissinger's method [17,18] and ΔH was assessed by integrating the area of the reaction peak and the interpolated baseline. A thermogravimetric analysis (TGA) was carried out to determine the quantity of O_2 released by the positive electrode on the NMC811 material charged at SOC 100 %. Then a 0D TR model was developed based on reaction rates equations [19,20]. The main reactions were the destabilization of the positive electrode which released O_2 and the formation of Li_2O. The goals of this model are to predict the TR behaviour of a Li|LLZO|NMC811 cell and to identify the key TR parameters. The key TR parameters are T_{ini}, T_{max}, the maximal pressure (P_{max}), the amount of gas released after condensation (n_{gas}), the energy released (E) and the duration of TR (d_{TR}). At the battery level, this model is compared with the TR behaviour of a Li|LLZO|NMC811 cell published previously [21]. This previous paper has shown that a 3 Ah Li|LLZO|NMC811 cell abuse by external heating lead to TR. It has be shown experimentally that $T_{ini} = 152 \pm 15$ °C, $T_{max} > 1{,}400$ °C, $P_{max} = 56 \pm 13$ bar, $E \approx 82$ kJ and $d_{TR} = 4 \pm 2$ ms [21]. Once the model has been validated, it can be used predictively in other configurations. For example, the quantity of lithium can be adjusted to quantify its impact on key TR parameters.

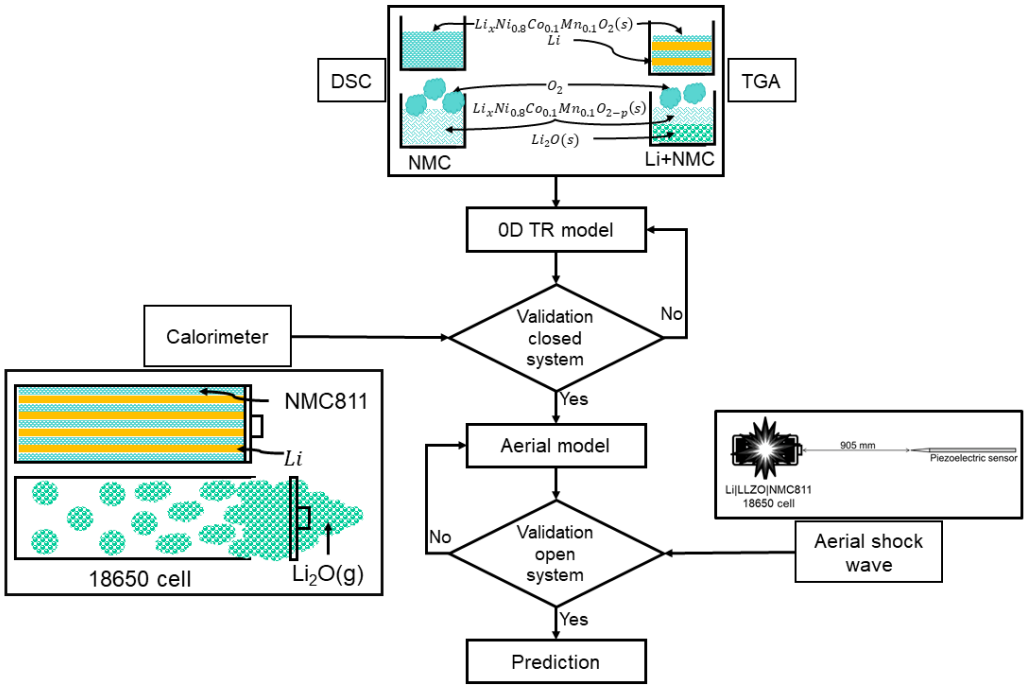

Figure 1: Experimental approach to assess the safety of the ASSB from DSC to a 0D TR model with an experimental validation.

Furthermore, this model is supplemented with an aerial model used to take into account the gases and their effect especially on shock wave formation. A shock wave is a sudden upsurge in temperature or in pressure due to an explosion or an object whose movement is faster than the speed of sound [22]. In our previous paper, it has be shown that a $3\ \mathrm{Ah}$ Li|LLZO|NMC811 cell abuse by external heating lead to TR which lead to the generation of a shock wave. The overpressure of $188\ \mathrm{mbar}$ was measured at a distance of $0.9\ \mathrm{m}$ for this cell and an equivalent mass of trinitrotoluene of $2.7\ \mathrm{g}$ ($m_{TNT,eq}$) was calculated [21].

To our knowledge, this study represents the first instance in which a model utilizing input data derived from the characterization of 5 to 10 milligrams of material (DSC) has successfully simulated the shock wave produced by the thermal runaway of a solid-state lithium battery with a capacity of several ampere-hours.

Methods:

1. Experimental methods

i) Powder preparation

Before the experiment, a commercial LG−HG2 cell at SOC $100\,\%$ was disassembled as presented in our previous article [23]. The amounts of oxygen and water of the glove box were lower than $0.1\ \mathrm{mg.\,L^{-1}}$. The powder of the positive electrode was recovered. This powder was washed 5 times with N-Methyl-2-pyrrolidone (NMP – Sigma – 328634) and 2 times with dimethyl carbonate (DMC – Sigma – 517127) to remove the remaining salt and binders such as polyvinylidene fluoride (pvdf). For the lithium, a $50\ \mu\mathrm{m}$ foil was used.

ii) TGA analysis

TGA analysis was performed in a NETZSCH STA 449F1 with a crucible made of Al_2O_3 (NETZSCH – GB445215). The temperature range was from 25 to $1{,}400\ °\mathrm{C}$ for each experiment. The heating rate was chosen as $10\ \mathrm{K.\,min^{-1}}$. TGA analysis was performed on NMC811 powder delithiated at SOC 100 %.

iii) DSC analysis

DSC analyses were carried out to characterize exothermic reactions and dissociate their contribution to the total heat released by the battery during TR.

Dynamic scanning experiments were conducted on a DSC 404 F1 Pegassus (NETZSCH) coupled with a type P sensor (DSC404F1A75.000-00). The temperature range was from 25 to $500\ °\mathrm{C}$ for each experiment. The heating rates (α) were chosen as 5, 10, 15 and $20\ \mathrm{K.\,min^{-1}}$. The crucibles used were made of $CrNi$ steel with a gold-plated surface (6.239.2-92.8.00) which can withstand about $100\ \mathrm{bar}$. “NETZSCH-Proteus-80” software was used to acquire, store and process the thermal curves. DSC analyses were performed on NMC811 powder delithiated at SOC $100\,\%$ and Li+NMC811 powders. These DSC analyses at different temperatures can be used to

determined E_a and A. E_a and A are the parameters used to characterize the reaction kinetics of thermal runaway.

2. Model framework:

Two models have been developed a 0D TR model and a blast wave model. COMSOL Multiphysics 6.0 is the software used for both models. The heat source has been provided by a system of ODEs based on reaction (1) to (7). COMSOL's free, generalized alpha time-step method is used with a relative tolerance of 10^{-8}.

i) 0D TR model

A 0D thermal runaway model has been developed for the Li|LLZO|NMC811 cell. This model considers two chemical reactions (Eq.(1) and Eq.(2)) which are respectively the destabilisation of the positive electrode $MO_2(s)$ (where M represents $Li_{0.28}Ni_{0.8}Co_{0.1}Mn_{0.1}$) and the formation of $Li_2O(g)$ [14,15]. As explained previously, a high-temperature TGA has been carried out an NMC811 powder between 25 and $1{,}400\ °C$. The quantity of oxygen released is $74\ \%$. This value may appear high and it is worth noting that, to the best of our knowledge, this is the first publication of a thermogravimetric analysis (TGA) conducted on NMC811 at such a high temperature. This measurement is significant as the amount of oxygen released plays a crucial role as the primary determinant in the runaway reactions of a lithium-ion cell. This model also considers five phase changes: lithium fusion/solidification (Eq.(3)), condensation/vaporisation and the fusion/solidification of Li_2O (Eq.(4) and Eq.(5)), aluminium fusion/solidification (Eq.(6)) and iron melting/freezing (Eq.(7)). The casing used is made with SPCE steel and a nickel coating. As the iron content of the casing is over $99\ \%$ wt, it was assumed to be composed of iron only. LLZO in contact with lithium is thermally stable up to $350\ °C$ [11]. Therefore LLZO is considered inert.

$$MO_2\ (s) \rightarrow MO_{0.52}(s) + 0.74\ O_2(g), \Delta H_1 \qquad (1)$$

$$Li(l) + \frac{1}{4}O_2(g) \rightarrow \frac{1}{2}Li_2O(g), \Delta H_2 \quad (2)$$

$$Li(s) \leftrightarrow Li(l), \Delta H_3 \quad (3)$$

$$Li_2O(g) \leftrightarrow Li_2O(l), \Delta H_4 \quad (4)$$

$$Li_2O(l) \leftrightarrow Li_2O(s), \Delta H_5 \quad (5)$$

$$Al(s) \leftrightarrow Al(l), \Delta H_6 \quad (6)$$

$$Fe(s) \leftrightarrow Fe(l), \Delta H_7 \quad (7)$$

The reaction rate r_i involves the reaction i, the mass of component j m_j (g), the partial order e_i, the cell temperature $T(\mathrm{K})$, the ideal gas constant R $(\mathrm{J.K^{-1}.mol^{-1}})$ and the two Arrhenius parameters: the activation energy E_a $(\mathrm{J.mol^{-1}})$ and the pre-exponential factor A $(\mathrm{s^{-1}})$ (Table S2 and S3). The destabilisation of the positive electrode, $MO_2(s)$ follows the reaction rate r_1 (Eq.(8)). The formation of $Li_2O(g)$ follows the reaction rate r_2 (Eq.(9)). The fusion/solidification of Li follows the reaction rate r_3 (Eq.(10)). It has been assumed that the other phase changes rates are proportional to the temperature differential. Eq.(11) and Eq.(12) are the reaction rates for the Li_2O condensation/vaporization and fusion/solidification. Equation (13) and(14) are the reaction rates for Al and Fe fusion/solidification, respectively. α_{Al} and α_{Fe} represent respectively the liquid aluminium mass fraction relative to the total mass of Al (m_{Al}) and the liquid iron mass fraction relative to the total mass of Fe (m_{Fe}), respectively.

$$r_1 = A_1 \exp\left(-\frac{E_{a_1}}{RT}\right) m_{MO_2}^{e_1} \quad (8)$$

$$r_2 = A_2 \exp\left(-\frac{E_{a_2}}{RT}\right) m_{Li(l)}^{e_2} \quad (9)$$

$$r_3 = A_3 \exp\left(-\frac{E_{a_3}}{RT}\right) m_{Li(s)}^{e_3} \quad (10)$$

$$r_4 = \beta_4\left(T_{Li_2O(l\leftrightarrow g)} - T\right) m_{Li_2O(g)} \quad (11)$$

$$r_5 = \beta_5\left(T_{Li_2O(s\leftrightarrow l)} - T\right)m_{Li_2O(l)} \quad (12)$$

$$r_6 = \beta_6\left(T_{Al(s\leftrightarrow l)} - T\right)m_{Al}\alpha_{Al} \quad (13)$$

$$r_7 = \beta_7\left(T_{Fe(s\leftrightarrow l)} - T\right)m_{Fe}\alpha_{Fe} \quad (14)$$

The species mass balances for MO_2, $MO_{0.52}$, $Li(s)$, $Li(l)$, O_2, $Li_2O(g)$, $Li_2O(l)$, $Li_2O(s)$, $Al(l)$, $Fe(l)$ are given by equations Eq.(15), Eq.(16), Eq.(17), Eq.(18), Eq.(19), Eq.(20), Eq.(21), Eq.(22), Eq.(23) and Eq.(24) respectively.

$$\frac{dm_{MO_2}}{dt} + r_1 = 0 \quad (15)$$

$$\frac{dm_{MO_{0.52}}}{dt} - r_1 = 0 \quad (16)$$

$$\frac{dm_{Li(s)}}{dt} + r_3 = 0 \quad (17)$$

$$\frac{dm_{Li(l)}}{dt} + r_2 - r_3 = 0 \quad (18)$$

$$\frac{dm_{O_2}}{dt} - 0.74\, r_1 + \frac{1}{4}r_2 = 0 \quad (19)$$

$$\frac{dm_{Li_2O(g)}}{dt} - r_2 + r_4 = 0 \quad (20)$$

$$\frac{dm_{Li_2O(l)}}{dt} - r_4 + r_5 = 0 \quad (21)$$

$$\frac{dm_{Li_2O(s)}}{dt} - r_5 = 0 \quad (22)$$

$$\frac{d\alpha_{Al}}{dt} + r_6 = 0 \quad (23)$$

$$\frac{d\alpha_{Fe}}{dt} + r_7 = 0 \quad (24)$$

The cell is heated from the outside with a temperature ramp of $6\,°\mathrm{C.min^{-1}}$ following the standard DO311 (Eq.(25)) [24]. The thermal flux $\dot{Q}_i$ of the two chemical reactions and the five phase changes are calculated from ΔH_i ($\mathrm{J.g^{-1}}$) and r_i (Eq.(26)). The cell temperature is calculated from the thermal balance equation Eq.(27) with

$m_{sl}(\mathrm{g})$ being the mass of the solid and liquid product, $c_p(\mathrm{J.K^{-1}.kg^{-1}})$: the isobaric heat capacity of the cell, $m_{gas}(\mathrm{g})$ the mass of the gaseous product, $c_{v_{gas}}(\mathrm{J.K^{-1}.kg^{-1}})$: the isochoric heat capacity of the gases, and $T_{gas}(\mathrm{K})$ the temperature of the gases, $S_c\ (\mathrm{m^2})$ the cell lateral surface, $h_c\ (\mathrm{W.m^{-2}.K^{-1}})$ the heat transfert coefficient between the cell and the air, ϵ_c the emissivity of the cell and $\sigma(\mathrm{W.m^{-2}.K^{-4}})$ the Stefan–Boltzmann constant (Table S4 and S5).

$$\frac{dT_{ext}}{dt} - Ramp = 0 \tag{25}$$

$$\dot{Q}_i = r_i \Delta H_i \tag{26}$$

$$\sum_{i=1}^{7} \dot{Q}_i + c_p \frac{dm_{sl}T}{dt} + \frac{dm_{gas}c_v T_{gas}}{dt} + S_c\left(h_c(T - T_{ext}) + \epsilon_c\, \sigma\, (T^4 - T_{ext}^4)\right) = 0 \tag{27}$$

The results of the TR model were used to estimate the pressure generated in the case where the cell is inserted in a closed vessel of volume $V_{vessel}(\mathrm{m^3})$ and thermally abused to generate a TR [21,23]. The pressure in the vessel $P(\mathrm{Pa})$ is calculated from the ideal gas law with $M_{gas}\ (\mathrm{g.mol^{-1}})$ the molar mass (Eq.(28)) (Table S1).

$$P = \frac{m_{gaz}RT_{cell}}{M_{gas}V_{calo}} \tag{28}$$

ii) Blast wave model

To describe the overpressure generated by the sudden gas release during the TR of the ASSB, a simple aerial explosive blast wave was developed. As presented by Esparza and Baker, the energy released E_{gas} in an assumed constant volume (confined explosion) is determined from the internal energy of the gases [25]. Due to the very fast reaction kinetics, adiabatic conditions were assumed. The internal energy of gases could be determined from Eq.(29) where $T_{max,C}(K)$ is the maximum combustion temperature, T_i the initial ambient temperature [22,25]. The equivalent

TNT mass $m_{eq,TNT}$ (kg) is deducted from Eq.(30) with $E_{1kg\,TNT}$(J) being the energy released by 1 kg of TNT (m_{1kg}).

On the basis of $m_{eq,TNT}$ *Kinney, G., and Graham, K.* establish a scaling law for explosive reactions in air [26]. Z is calculated from the actual distance from the centre of the explosion d and the equivalent TNT mass (Eq.(31)). The peak overpressure P^0 is linked to the scaled distance Z and the atmospheric pressure P_a by Eq(32)) [26].

$$E_{gas} = m_{gas} c_{v_{gas}} (T_{max,C-} - T_i) \quad (29)$$

$$m_{eq,TNT} = \frac{E_{gas}}{E_{1g\,TNT}} m_{1kg} \quad (30)$$

$$Z = \frac{d}{m_{eq,TNT}^{\frac{1}{3}}} \quad (31)$$

$$\frac{P^0}{P_a} = \frac{808\left[1 + \left(\frac{Z}{4.5}\right)^2\right]}{\sqrt{1 + \left(\frac{Z}{0.048}\right)^2}\sqrt{1 + \left(\frac{Z}{0.32}\right)^2}\sqrt{1 + \left(\frac{Z}{1.35}\right)^2}} \quad (32)$$

Results:

1. TGA and DSC analysis

TGA analysis was performed on NMC811 powder delithiated at SOC 100 %. Between 25 and 1,400 °C, the mass loss of NMC811 was 27 % (Figure 2). By assuming that the mass loss of NMC811 powder was due only to the release of O_2 (Eq.(1)) then the mass loss of O_2 was about 74 % (Figure 2).

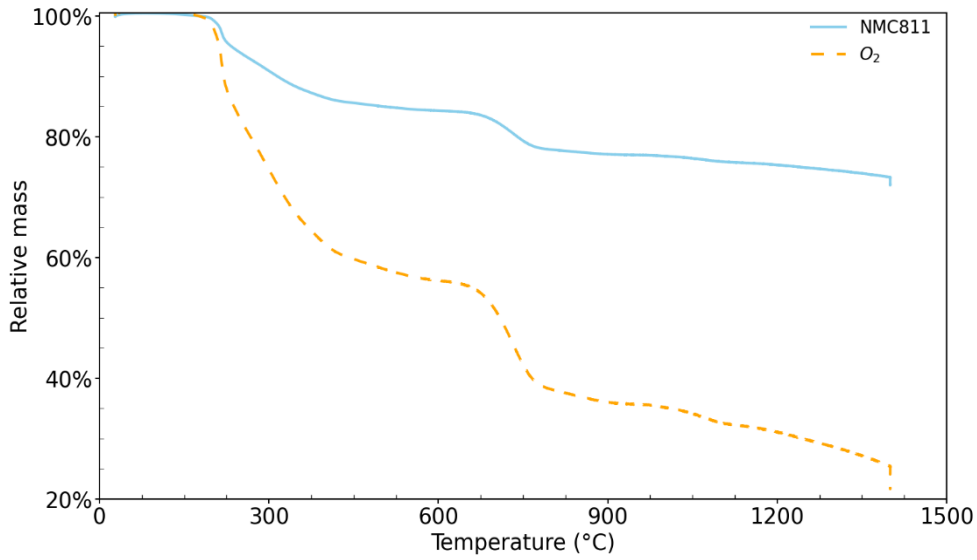

Figure 2: Relative mass of NMC811 powder delithiated at SOC $100\,\%$ *as a function of temperature ranging from* 25 *to* $1{,}400\,°C$

DSC analyses were performed on NMC811 powder delithiated at SOC $100\,\%$. The NMC811 showed two exothermic peaks at $230\,°\mathrm{C}$ and at $390\,°\mathrm{C}$ (Figure 3 – a). The DSC analyses on Li-metal and NMC811 powder at SOC $100\,\%$ showed an endothermic peak at $187\,°\mathrm{C}$, which corresponded to lithium fusion. They also showed two exothermic peaks at $230\,°\mathrm{C}$ and $385\,°\mathrm{C}$ (Figure 3 – b).

The kinetics parameters can be deducted by fitting DSC profiles at variable heating rates. Kissinger's method [18] was applied to assess the pre-exponential factor (A) and the activation energy (E_a) without taking into account the mechanism function. Kissinger's equation (Eq.(33)) [17,18] is based on the variation of the peak temperature: $T_{p,j}\ (\mathrm{K})$ as function of the heating rate: $\alpha_j\ (\mathrm{K.\,min^{-1}})$ with u is the number of variable heating rates. The pre-exponential factor (A) can be deduced from the ordinate straight line and the activation energy (E_a) can be deduced from the straight line fitting (Figure 3 – c and d). The kinetics parameters are listed

Table 1. For the melting of Li, the Kissinger parameters used are those deduced from the Li+NMC left peak (Eq.(10)). The Kissinger parameters used for the two

chemical reactions (Eq.(1) and Eq.(2)) are those from the peak at $400\ °C$ because they were obtained with the highest temperature. Therefore, the NMC right peak was used for the destabilisation of the NMC811 (Eq.(8)) and Li+NMC right peak was used for the formation of $Li_2O(g)$ (Eq.(9)).

$$\ln\left(\frac{\alpha_j}{T_{p,j}^2}\right) = \ln\left(\frac{AR}{Ea}\right) - \frac{Ea}{RT_{p,j}} \text{ with } j \in [\![1, u]\!] \qquad (33)$$

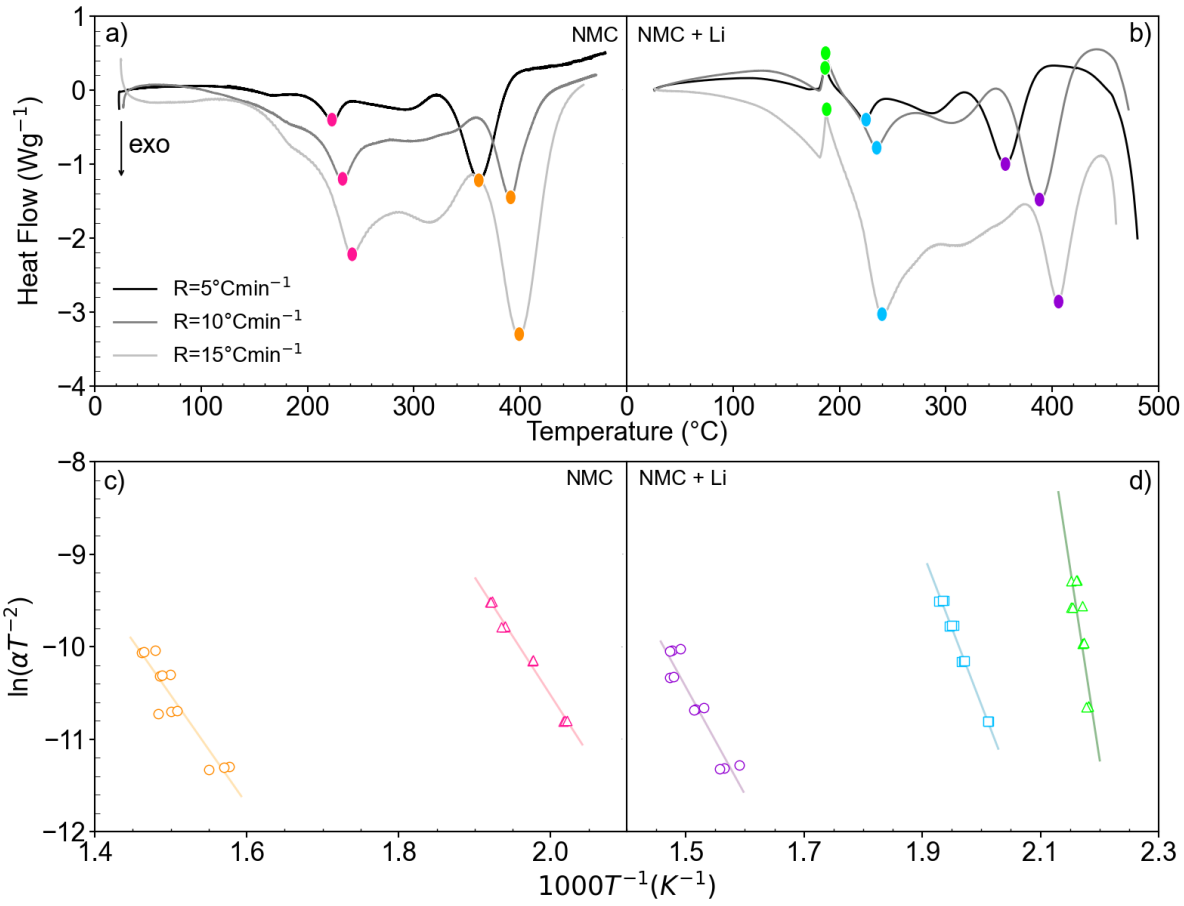

Figure 3 : DSC at different ramp temperatures 5, 10 *and* $15\ K.min^{-1}$ *a) NMC811 and b)* Li *+ NMC811. Kissinger regression c) NMC811 and d)* Li *+ NMC811.*

Table 1: Kinetics parameters of NMC811 and Li *+ NMC811 delithiated at SOC* $100\ \%$.

	$E_a(\mathrm{J.mol^{-1}})$	$A(\mathrm{s^{-1}})$
NMC left peak	$1.06\ 10^6$	$4.29\ 10^{10}$
NMC right peak	$9.79\ 10^4$	$1.47\ 10^7$
Li+NMC left peak	$3.45\ 10^5$	$2.29\ 10^{39}$
Li+NMC middle peak	$1.38\ 10^5$	$1.12\ 10^{14}$

Li+NMC right peak	$9.66\ 10^{4}$	$1.26\ 10^{7}$

1

2 2. Thermal runaway model results

3 The first goal of this model was to characterise the TR of the Li|LLZO|NMC811
4 cell. This model predicted the degradation reactions, phase change, gas generation
5 and internal temperature evolutions of the cell studied. Three stages govern TR. At the
6 start, the cell was heated with a temperature ramp of $6\ °C.\min^{-1}$ (Figure 4 – heating)
7 [24]. Therefore, the temperature increased linearly until T_{ini}, here $180\ °C$. When this
8 temperature was reached, TR took place (Figure 4 – TR). The temperature increases
9 sharply to T_{max} here $2{,}470\ °C$. At this moment, two gases were released: $Li_2O(g)$ and
10 O_2. A temperature plateau was observed until the condensation of Li_2O. After TR, the
11 cell was cooled by radiation and natural convection and the temperature decreased
12 until it reached the ambient temperature (T_{amb}) (Figure 4 – cooling). Two temperature
13 plateaux were observed at $1{,}570$ and $1{,}536\ °C$, corresponding to the solidification of
14 Li_2O and then Fe.

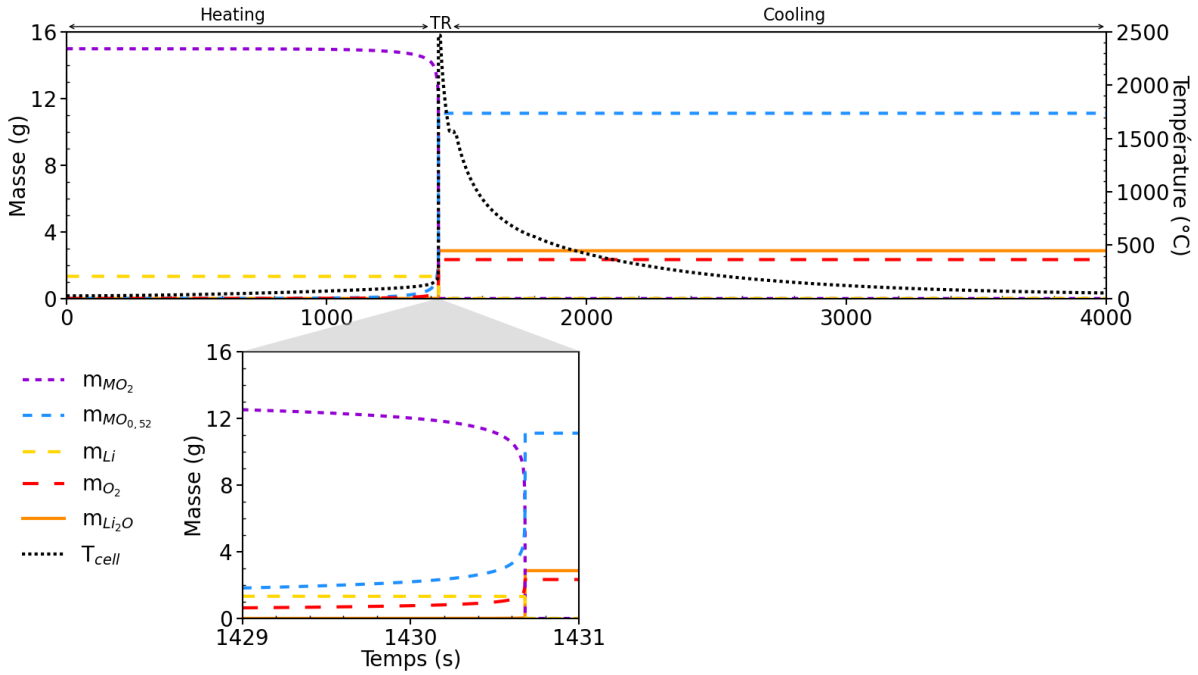

Figure 4: Evolutions of masses of MO_2, $MO_{0.52}$, O_2, Li and Li_2O coupled with the internal cell temperature evolution of the Li|LLZO|NMC811 cell at SOC $100\ \%$.

In this model, the energy released during TR was $77\ \mathrm{kJ}$ and the duration of TR was $6\ \mathrm{ms}$. Taking into account a closed $0.538\ \mathrm{L}$ vessel, the pressure released by the cell was $46\ \mathrm{bar}$.

3. Blast wave model results

Based on the energy released by the gas mixture composed of $73\ \mathrm{mmol}$ of O_2 and $96\ \mathrm{mmol}$ of $Li_2O(g)$, the maximal energy released by the gases was $12.9\ \mathrm{kJ}$, corresponding to an equivalent TNT mass of $3.0\ \mathrm{g}$. At a physical distance of $0.9\ \mathrm{m}$ from the cell, the scaled distance was $6.18\ \mathrm{m.kg^{-1/3}}$ and the peak overpressure is $199\ \mathrm{mbar}$.

4. Comparison of the TR model and blast wave model results with experiments

The results of the model are compared with the values of two different experiments described in detail in our previous article [21]. The first experiment consisted of initiating the thermal runaway of a cell reassembled in a closed calorimeter. This first experiment provided all the values in Table 2 except the peak overpressure $P^0_{0.9m}$ and the equivalent TNT mass $m_{TNT,eq}$. In order to measure the

overpressure and deduce the TNT mass equivalent, a second experiment was carried out in the open-air area.

The initiation temperature obtained experimentally was lower than that obtained by the model. This is reasonable because experimentally the temperature measured was the surface temperature while the temperature deduced from TR model was the internal temperature. It is well-known that there is a temperature gradient between the centre and the periphery [23,27]. Unfortunately, the maximal temperature of this cell could not be recorded. However, as the casing made of iron melted, we can conclude that the maximal temperature was at least $1{,}400\,°\mathrm{C}$; this is consistent with the calculated temperature of $2{,}470\,°\mathrm{C}$ (Table 2). The P_{max}, E and d_{TR} obtained with this model were in the confidence interval determined experimentally (Table 2).

The relative errors between the experimental and model values were about $10\,\%$ and $6\,\%$ for $m_{TNT,eq}$ and $P^{0}_{0.9m}$ respectively (Table 2). These differences can be explained by the fact that not all the gases were used to generate a shock wave. The kinetic energy transferred to the solids and support device was not taken into account, nor was the energy required to deform and break the casing and support device. The 0D TR model was congruent with the experiments performed on the Li|LLZO|NMC811 cell.

5. Prediction for an anode less ASSB.

Lithium reacts violently with oxygen. One solution for improving the safety of the lithium-metal ASSB is to reduce the amount of lithium so only the quantity required to cycle the cell is available. This technology is named anode-less.

Our TR model and blast wave model were applied to simulate an anode-less ASSB. Numerically, T_{ini} is similar and T_{max} is lower for the anode-less technology than for the cell with excess Li (Table 2). This means that the thermal runaway of anode-

less technology starts at the same temperature, however the maximum temperature reached is lower. The energy released is lower for the anode-less technology than for the cell with Li excess. The lower temperature and lower energy released means that the risk of TR propagation could be reduced with the anode-less technology. P_{max}, $m_{TNT,eq}$ and $P_{0.9m}^{0}$ are lower for the anode-less technology than in the cell with excess Li. This could mean that structural damage on the casing and pack could be lower. d_{TR} is comparable for both technologies.

Table 2: TR parameters: T_{ini}, T_{max}, E, d_{TR}, P_{max} and n_{gas} for TR of a Li|LLZO|NMC811 cell obtained numerically and experimentally [21].

	T_{ini} (°C)	T_{max} (°C)	P_{max} (bar)	E (kJ)	d_{TR} (ms)	$m_{TNT,eq}$ (g)	$P_{0.9m}^{0}$ (mbar)
Quantity of Li in experiment same as state of art	152 ± 15	$> 1{,}400$	56 ± 13	82	4 ± 2	2.7	188
Quantity of Li in model same as state of art	180	2,470	45	77	6	3.0	199
Anode less model	180	2,039	36	52	6	2.0	161

6. Reaction path for Li|LLZO|NMC811

The TR of Li|LLZO|NMC811 is divided in three stages. First, O_2 is released from NMC811 and the lithium-metal is melted from $180\,°C$ (Figure 5 – I). $18\,kJ$ where released during this stage. Then, O_2 and the lithium-metal react together by forming $Li_2O(g)$ (Figure 5 – II) followed immediately by its condensation (Figure 5 – III). Respectively, $19\,kJ$ and $34\,kJ$ are released during these stages. In the cooling phase, $6\,kJ$ are additionally released link to the solidification of Li_2O (Eq. (5)).

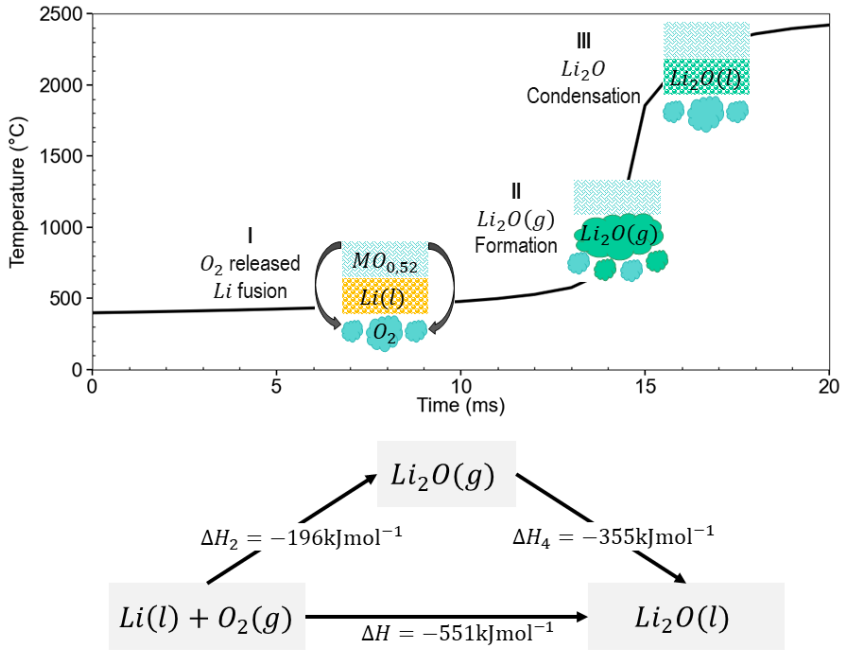

Figure 5 : Reaction path for Li|LLZO|NMC811 cell during TR.

Discussion:

The first step was to determine the input parameters required for this TR model. DSC analyses were carried out on NMC811 and Li+NMC811 materials in order to obtain kinetic parameters. TGA analysis was performed on the NMC811 material to obtain the quantity of oxygen released by the positive electrode. The reassembled Li|LLZO|NMC811 cell used the LG model HG2 (LG−HG2) positive electrode. *Ante-mortem* analysis were performed on the LG−HG2 positive electrode to know the amount of NMC811 and aluminium in the Li|LLZO|NMC811 cell. The coating of LLZO was home-made so its amount was known. The amount of lithium and iron were known because they were weighed beforehand. The other parameters defined from the literature were more fundamental parameters such as the specific heat of the materials and the melting temperatures.

The second step consisted in developing a 0D TR model. It was mainly based on two chemical reactions: the destabilisation of the NMC811 positive electrode (Eq.(1)) and the reaction between $Li(l)$ and $O_2(g)$ which formed $Li_2O(g)$ (Eq.(2)). This

model was essentially established on two balances: the species mass balance (Eq.(15) to Eq.(24)) and the thermal balance (Eq.(27)). The end of this stage involved the comparison of TR parameters: T_{ini}, T_{max}, P_{max}, n_{max}, E and d_{TR} obtained experimentally and numerically. The TR model was congruent with the experiments. The maximum reaction temperature could not be measured because thermocouple measurements are relevant only up to $1{,}400\,°\mathrm{C}$. However, the two concordant predictions and measurements (P_{max} and E) suggest that the model's prediction of T_{max} ($2{,}470\,°\mathrm{C}$) was reasonable.

The third stage consisted in developing an aerial blast wave model. The goal was to determine the energy released by the gases: $O_2(g)$ and $Li_2O(g)$ during TR (Eq.(29)). Knowing that $1\,\mathrm{g}$ of TNT is equivalent to $4.184\,\mathrm{kJ}$, the mass of equivalent TNT was determined for the Li|LLZO|NMC811 cell. Then, using the Kinney and Graham law (Eq.(32)), the aerial overpressure at $0.9\,\mathrm{m}$ was deducted. To validate this model, the $m_{TNT,eq}$ and $P^0_{0.9m}$ parameters were compared to those obtained experimentally. The aerial overpressure model was congruent with the experiments. Furthermore, the corresponding $m_{eq,TNT}$ predictions and measurements suggests also that the model's prediction of T_{max} ($2{,}470\,°\mathrm{C}$) was very close to reality, because from equation (29) the energy of the gas was calculated directly from the maximum temperature of the reaction. To our knowledge, this is the first model which, based on the intrinsic characterisation of active cell materials, predicts very rapid reaction kinetics (a few milliseconds). As this reaction is very rapid, a shock wave was formed. Our blast wave model enabled us to quantify the overpressure. This was well suited to experiments on a cell of several Ah.

For the cell tested experimentally and numerically, the amount of lithium was representative of current cells, although in excess. One way of optimising it was to

have only the amount of lithium needed for the cell cycle. This was the prediction step. Reducing the amount of lithium helped to increase the safety of the cell. In the anode-less case, the temperature T_{ini} was the same. T_{max} and E decreased which have limited the TR propagation risk. P_{max}, $m_{TNT,eq}$ and $P^{0}_{0.9m}$ decreased which could have limited the structural damage on the casing and pack. Thus, the results of the anode-less cells showed that developing this technological solution will also improve safety. Nevertheless, this will not be enough to ensure that these cells are safe.

More generally, the maximum temperatures reached by all-solid state cells are much higher than those reached by cells with a graphite anode and liquid electrolyte. The high temperatures reached by all-solid state cells during thermal runaway can be explained by the reduction in cell mass due in part to the removal of graphite, but it can also be explained by the higher mass enthalpy of the formation of Li_2O. Unlike carbon combustion, where CO_2 remains in the form of a gas. As Figure 5 shows, the latent heat of vaporization and condensation of Li_2O acts as an attractor and a threshold at the phase change temperature. As presented by *M. Shiemann and al*, the temperature of lithium fire is limited by the effects of decomposition, melting and boiling [28]. In the case of our model, it was mostly the boiling of Li_2O that limited the maximum temperature of thermal runaway. It is interesting to note that the flame temperature of lithium in oxygen is close to the maximum temperature proposed by the model in Table 2. This is easily explained, as the reactions are the same: lithium and oxygen released by the cathode gives Li_2O. Furthermore, the phenomenon limiting the maximum temperature was also the vaporisation of Li_2O in both cases. In a slightly different case, sulphide electrolyte also exhibit thermal runaway reactions that can reach temperatures of around $2{,}500\ ℃$ [12].

The high temperatures induced by the lithium fire accelerate the reaction rate and increase the internal energy of the gases, which plays a crucial role in the creation of a shock wave when an all-solid cell is subject to runaway. In the future, the challenge will undoubtedly to limit this maximum temperature, to ensure the safety of all-solid state batteries.

Conclusion

In this study, a thermal runaway model for an all-solid cell was proposed. The construction of this model (input data) was mainly based on experiments (DSC, TGA). In order to improve the accuracy of the amount of oxygen released by the cathode, a TGA up to $1{,}400\,°C$ had to be carried out, which to our knowledge had never been published before for an NMC811.

Only the fundamental data, such as specific capacity and reaction enthalpies, were taken from the literature.

This materials-scale characterisation approach enabled us to propose a robust model that predicts the runaway of Li|LLZO|NMC811 cells in a closed calorimeter with good accuracy. The calculated key parameters such as the initiation temperature T_{ini}, maximum pressure $P_{\max}$, the energy released by the thermal runaway E and its duration d_{TR} were in good agreement with the experimental data. In addition, this model calculated the blast wave over pressure produced by the thermal runaway of this cell in an open area condition.

For the first time, the thermal runaway of an all-solid-state Li|LLZO|NMC811 cell and the blast wave overpressure have been modelled in good agreement. This shows that the mechanisms leading to the thermal runaway of ASSB and their possible consequences out of the cell are progressively better understood. In addition, the

simulation of a cell using anode-less technology showed that even with the minimum quantity of lithium, the thermal runaway, while reduced, remained significant.

In addition, this work highlighted the impact of the oxygen released by the cathode, its strong reaction with the lithium during TR, and the subsequent blast wave overpressure caused by the gases generated. The safety of solid-state batteries, often seen as the holy grail of batteries, is still an open question and further research, strongly coupled with technological developments is needed.

Authors' contribution

J.C: conceptualization, methodology, software, validation, formal analysis, writing original draft, writing review and editing and visualisation. A.B: methodology, validation, resources and writing review and editing. P-X.T: validation and writing review and editing. R.V: conceptualization, validation, resources, writing original draft, writing review and editing and supervision.

Acknowledgments:

The authors would like to express their gratitude for the technical support provided by Sorana Luca for the TGA analysis and Sylvie Genies for the ante-mortem analysis. We also would like to thanks Sergey Kudriakov for the technical discussion about shoke waves.

Conflict of Intersement statement :

The authors declare no conflict of interest.

Data availability statement:

The data that support the findings of this study are available on request from the corresponding author. The data are not publicly available due to privacy or ethical restrictions.

References:

[1] Nitta N, Wu F, Lee JT, Yushin G. Li-ion battery materials: present and future. MaterialsToday 2015;18:252–264. https://doi.org/https://doi.org/10.1016/j.mattod.2014.10.040.

[2] Tian X, Yi Y, Fang B, Yang P, Wang T, Liu P, et al. Design Strategies of Safe Electrolytes for Preventing Thermal Runaway in Lithium Ion Batteries. Chemistry Materials 2020;32:9821–9848. https://doi.org/10.1021/acs.chemmater.0c02428.

[3] Wang Q, Ping P, Zhao X, Chu G, Sun J, Chen C. Thermal runaway caused fire and explosion of lithium ion battery. Journal Power Sources 2012;208:210–224. https://doi.org/https://doi.org/10.1016/j.jpowsour.2012.02.038.

[4] Zalosh R, Gandhi P, Barowy A. Lithium-ion energy storage battery explosion incidents. Journal Loss PreventionProcessIndustries 2021;72:104560. https://doi.org/https://doi.org/10.1016/j.jlp.2021.104560.

[5] Tian Y, Zeng G, Rutt A, Shi T, Kim H, Wang J, et al. Promises and Challenges of Next-Generation “Beyond Li-ion” Batteries for Electric Vehicles and Grid Decarbonization. ChemicalReviews 2021;121:1623–1669. https://doi.org/10.1021/acs.chemrev.0c00767.

[6] Kim S, Chart YA, Narayanan S, Pasta M. Thin Solid Electrolyte Separators for Solid-State Lithium–Sulfur Batteries. NanoLetters 2022;22:10176–10183. https://doi.org/10.1021/acs.nanolett.2c04216.

[7] Albertus P, Anandan V, Ban C, Balsara N, Belharouak I, Buettner-Garrett J, et al. Challenges for and Pathways toward Li-Metal-Based All-Solid-State Batteries. ACSEnergyLetters 2021;6:1399–1404. https://doi.org/10.1021/acsenergylett.1c00445.

[8] Huo J H. Jiang M. Bai Y. Ahmed S. Volz K. Hartmann H. Henss A. Singh C. V. Raabe D. Janek. Chemo-mechanical failure mechanisms of the silicon anode in solid-state batteries. NatMater 2024. https://doi.org/https://doi.org/10.1038/s41563-023-01792-x.

[9] Lv Y, Huang S, Zhao Y, Roy S, Lu X, Hou Y, et al. A review of nickel-rich layered oxide cathodes: synthetic strategies, structural characteristics, failure mechanism, improvement approaches and prospects. AppliedEnergy 2022;305:117849. https://doi.org/https://doi.org/10.1016/j.apenergy.2021.117849.

[10] Inoue T, Mukai K. Are All-Solid-State Lithium-Ion Batteries Really Safe?–Verification by Differential Scanning Calorimetry with an All-Inclusive Microcell. ACSAppliedMaterials&Interfaces 2017;9:1507–1515. https://doi.org/10.1021/acsami.6b13224.

[11] Chen R, Nolan AM, Lu J, Wang J, Yu X, Mo Y, et al. The Thermal Stability of Lithium Solid Electrolytes with Metallic Lithium. Joule 2020;4:812–821. https://doi.org/https://doi.org/10.1016/j.joule.2020.03.012.

[12] Wu Y, Xu J, Lu P, Lu J, Gan L, Wang S, et al. Thermal Stability of Sulfide Solid Electrolyte with Lithium Metal. AdvancedEnergyMaterials 2023;n/a:2301336. https://doi.org/https://doi.org/10.1002/aenm.202301336.

[13] Kim T, Kim K, Lee S, Song G, Jung MS, Lee KT. Thermal Runaway Behavior of Li6PS5Cl Solid Electrolytes for LiNi0.8Co0.1Mn0.1O2 and LiFePO4 in All-Solid-State Batteries. Chemistry Materials 2022;34:9159–9171. https://doi.org/10.1021/acs.chemmater.2c02106.

[14] Bates AM, Preger Y, Torres-Castro L, Harrison KL, Harris SJ, Hewson J. Are solid-state batteries safer than lithium-ion batteries? Joule 2022;6:742–755. https://doi.org/https://doi.org/10.1016/j.joule.2022.02.007.

[15] Johnson N, Albertus P. Modeling Thermal Behavior and Safety of Large Format All-Solid-State Lithium Metal Batteries under Thermal Ramp and Short Circuit Conditions. Journal The Electrochemical Society 2022;169:060546. https://doi.org/10.1149/1945-7111/ac79cf.

[16] Ouyang D, Weng J, Chen M, Zhu Y, Wang J, Wang Z. A comparative study on safety and electrochemical characteristics of cylindrical lithium-ion cells with various formats. ProcessSafety Environmental Protection 2022;161:126–135. https://doi.org/https://doi.org/10.1016/j.psep.2022.03.027.

[17] Ren D, Liu X, Feng X, Lu L, Ouyang M, Li J, et al. Model-based thermal runaway prediction of lithium-ion batteries from kinetics analysis of cell components. AppliedEnergy 2018;228:633–644. https://doi.org/https://doi.org/10.1016/j.apenergy.2018.06.126.

[18] Kissinger HE. Variation of Peak Temperature with Heating Rate in Differential Thermal Analysis. Journal ResearchNationalBureau Standards 1956;57:217–221. https://doi.org/http://dx.doi.org/10.6028/jres.057.026.

[19] Hatchard TD, MacNeil DD, Basu A, Dahn JR. Thermal Model of Cylindrical and Prismatic Lithium-Ion Cells. Journal The Electrochemical Society 2001;148:A755. https://doi.org/10.1149/1.1377592.

[20] Spotnitz R, Franklin J. Abuse behavior of high-power, lithium-ion cells. Journal Power Sources 2003;113:81–100. https://doi.org/https://doi.org/10.1016/S0378-7753(02)00488-3.

[21] Charbonnel J, Dubourg S, Testard E, Broche L, Magnier C, Rochard T, et al. Preliminary study of all-solid-state batteries: evaluation of blast formation during the thermal runaway. iScience 2023:108078. https://doi.org/https://doi.org/10.1016/j.isci.2023.108078.

[22] Ramamurthi K. Modeling explosions and blast wave. Springer India 2nd edn; 2021. https://doi.org/10.1007/978-3-030-74338-3_3.

[23] Charbonnel J, Darmet N, Deilhes C, Broche L, Reytier M, Thivel P-X, et al. Safety Evaluation of All-Solid-State Batteries: An Innovative Methodology Using In Situ Synchrotron X-ray Radiography. ACSAppliedEnergyMaterials 2022;5:10862–10871. https://doi.org/https://doi.org/10.1021/acsaem.2c01514.

[24] RTCA Minimum Operational Performances Standards for Rechargeable Lithium Battery and Battery Systems (DO-311). Washington,DC: RTCA DO-311; 2017.

[25] Esparza ED, Baker WE. Measurements of Blast Waves from Bursting Frangible Spheres Pressurized with Flash-Evaporating Vapor or Liquid. National Aeronautics and Space Administration; 1977.

[26] Kinney G, Graham K. Explosive shocks in air (2nd edition). Berlin New York, Springer-Verlag, 1985, 282 p 1985;-1.

[27] Dai H, Jiang B, Wei X. Impedance Characterization and Modeling of Lithium-Ion Batteries Considering the Internal Temperature Gradient. Energies 2018;11. https://doi.org/10.3390/en11010220.

[28] Schiemann M, Bergthorson J, Fischer P, Scherer V, Taroata D, Schmid G. A review on lithium combustion. AppliedEnergy 2016;162:948–965. https://doi.org/https://doi.org/10.1016/j.apenergy.2015.10.172.